

Pratik Mukherjee, MD, PhD  
Mark M. Bahn, MD, PhD  
Robert C. McKinstry, MD,  
PhD  
Joshua S. Shimony, MD, PhD  
Thomas S. Cull, PhD  
Erbil Akbudak, PhD  
Abraham Z. Snyder, MD, PhD  
Thomas E. Conturo, MD, PhD

### Index terms:

Anisotropy  
Brain, diffusion, 10.12144, 10.92  
Brain, gray matter, 10.92  
Brain, infarction, 10.78  
Brain, MR, 10.121411, 10.121413,  
10.121416, 10.12144  
Brain, white matter, 10.92  
Diffusion tensor  
Magnetic resonance (MR), diffusion  
study, 10.12144, 10.92  
Magnetic resonance (MR), rapid  
imaging, 10.121413

Radiology 2000; 215:211–220

### Abbreviations:

$A_r$  = diffusion anisotropy  
ADC = apparent diffusion coefficient  
 $\bar{D}$  = isotropic diffusion coefficient  
FLAIR = fluid-attenuated inversion  
recovery  
ROI = region of interest

<sup>1</sup> From the Mallinckrodt Institute of Radiology, Washington University School of Medicine, 510 S Kingshighway Blvd, St Louis, MO 63110. Received January 19, 1999; revision requested March 9; final revision received July 15; accepted July 20. This work was supported by the Major Grants Program of the McDonnell Center for Higher Brain Function and the Charles A. Dana Foundation Consortium on Neuroimaging Leadership Training and National Institutes of Health grant NS06833. Address reprint requests to P.M. (e-mail: MukherjeeP@mir.wustl.edu).

© RSNA, 2000

### Author contributions:

Guarantors of integrity of entire study, P.M., M.M.B., T.E.C.; study concepts, P.M., M.M.B., R.C.M., J.S.S., T.E.C.; study design, P.M., M.M.B., T.E.C.; definition of intellectual content, P.M., M.M.B., R.C.M., J.S.S., A.Z.S., T.E.C.; literature research, P.M., R.C.M.; clinical studies, P.M., M.M.B.; data acquisition, P.M., E.A.; data analysis, R.C.M., J.S.S., T.S.C., A.Z.S., E.A., T.E.C.; statistical analysis, P.M., M.M.B., A.Z.S., T.E.C.; manuscript preparation, P.M.; manuscript editing and review, P.M., M.M.B., R.C.M., J.S.S., A.Z.S., T.E.C.

# Differences between Gray Matter and White Matter Water Diffusion in Stroke: Diffusion-Tensor MR Imaging in 12 Patients<sup>1</sup>

**PURPOSE:** To investigate differences in water diffusion between white matter and gray matter in acute to early subacute stroke with diffusion-tensor magnetic resonance (MR) imaging.

**MATERIALS AND METHODS:** Twelve patients with unilateral middle cerebral arterial infarcts were examined with diffusion tensor-encoded echo-planar MR imaging 17 hours to 5 days after stroke onset. Isotropic diffusion coefficient ( $\bar{D}$ ) and diffusion anisotropy ( $A_r$ ) images were computed.  $\bar{D}$  values were measured in ischemic and contralateral gray matter and white matter by using  $A_r$  images to differentiate white matter from gray matter.  $\bar{D}$  images were compared with unidirectional and directionally averaged diffusion-weighted images.

**RESULTS:** In all patients,  $\bar{D}$  images showed two distinct levels of diffusion reduction in the infarct; more severe reduction occurred exclusively in white matter.  $\bar{D}$  values were significantly less in infarcted white matter than in infarcted gray matter, whereas  $\bar{D}$  values in the contralateral white matter and gray matter were not significantly different. Relative to the contralateral side,  $\bar{D}$  values in the infarct were reduced by 46% in white matter and by 31% in gray matter ( $P < .001$ ). Diffusion-weighted imaging caused underestimation of the magnitude and, in some cases, the spatial extent of the white matter diffusion abnormality.

**CONCLUSION:** Isotropic diffusion is more reduced in white matter than in gray matter in acute to early subacute middle cerebral arterial stroke. Diffusion-tensor imaging may be more sensitive than diffusion-weighted imaging to white matter ischemia.

Diffusion-weighted magnetic resonance (MR) imaging has proved to be a valuable clinical tool in the assessment of stroke because of its high sensitivity in the hyperacute period when thrombolytic therapy may be effective (1) and because of its ability to distinguish acute infarcts from chronic infarcts (2–4). However, contrast on diffusion-weighted images is confounded by T2-weighted, spin-density, and T1-weighted signal effects and by the orientation of white matter fibers (5). Hence, diffusion-weighted imaging alone cannot provide quantitative diffusion information in stroke (6).

Most of the quantitative diffusion data available in the clinical stroke literature are based on determinations of the effective or apparent diffusion coefficient (ADC) along the direction of a single diffusion-sensitizing gradient. Unidirectional ADC images of this type contain uncontrolled intensity variations due to anisotropic diffusion along white matter fibers. The ADC can also be measured along three orthogonal gradients and averaged to compensate for the effects of anisotropy. Studies based on this averaged orthogonal approach have not revealed appreciable differences between gray matter and white matter diffusion in acute stroke (7–9).

However, the detection of these diffusion differences may be limited by factors such as a low signal-to-noise ratio, eddy current-induced image misregistration, anatomic distur-

tions in the infarct, and small infarct size. It is important to further examine the issue of diffusion in ischemic gray versus white matter because the results may affect interpretation of the radiologic image, clinical treatment of patients with stroke, clinical studies of neuroprotective agents, and basic scientific studies of infarct heterogeneity and the pathophysiologic mechanisms of stroke.

We conducted this investigation to determine if differences in water diffusion exist between white matter and gray matter in acute to early subacute human stroke with use of optimized tetrahedral-orthogonal diffusion-tensor imaging with image realignment (10,11). This method is used to sample the diffusion tensor along four tetrahedral and three orthogonal directions and may offer advantages for the detection of diffusion differences in gray matter and white matter. Tetrahedral or combined tetrahedral-orthogonal encoding provides a higher signal-to-noise ratio than does orthogonal encoding alone (12).

In addition, we used the anisotropy information available from diffusion-tensor imaging to distinguish white matter from gray matter, even in cases of distorted anatomy, facilitating comparisons between the two tissue types. We also compared diffusion-tensor imaging with diffusion-weighted imaging to assess the diffusion abnormality within gray matter and white matter in stroke. Finally, we gauged the extent to which T2-weighted signal effects contribute to the observed disparities between diffusion-weighted and diffusion-tensor imaging.

## MATERIALS AND METHODS

### Data Acquisition

We performed a retrospective study of diffusion-weighted and diffusion-tensor imaging data in 12 consecutive patients (four men, eight women; age range, 30–90 years; mean age, 65 years [Table 1]) with stroke during an 18-week period. Data were obtained as part of a routine clinical protocol for MR imaging of stroke. The inclusion criterion was the presence of a medium to large unilateral nonhemorrhagic middle cerebral arterial infarct that involved confluent areas of white matter and gray matter on unidirectional diffusion-weighted images.

All patients were imaged within 5 days of symptom onset. This period encompasses the acute to early subacute stages of infarction and was chosen because

**TABLE 1**  
Patient Demographics and Stroke Characteristics

Patient No./ Age (y)/Sex	Age of Infarct	Infarct Group (d)	Infarct Area* (No. of pixels)	Infarct Location in the Middle Cerebral Arterial Territory
1/71/F	46 h	<3	1,786	Left anterior
2/53/M	84 h	3–5	1,752	Left anterior
3/54/F	17 h	<3	1,496	Right anterior
4/81/M	4 d	3–5	1,539	Left posterior
5/41/F	5 d	3–5	2,938	Left posterior
6/76/F	5 d	3–5	5,141	Left
7/30/F	26–38 h	<3	2,529	Left
8/61/M	3–4 d	3–5	3,958	Left
9/90/F	24–48 h	<3	3,502	Right anterior
10/87/F	3–4 d	3–5	1,817	Right posterior
11/80/M	36–48 h	<3	1,018	Left anterior
12/59/F	24–48 h	<3	751	Right temporal and insular

\* Infarct area in the representative transverse section.

diffusion changes in stroke pseudonormalize within 6–7 days (13). The earliest infarct in this series of patients occurred at 17 hours after symptom onset. Data from earlier periods of stroke were not available, as MR imaging data are not routinely obtained on the first day after symptom onset at our institution. Because susceptibility effects from blood products confound diffusion measurements, patients were excluded who had MR imaging evidence of hemorrhage in the region of infarction as determined with T2\*-weighted echo-planar imaging.

Six patients were imaged within 72 hours of symptom onset (range, 17–48 hours), and the other six patients were examined 3–5 days after symptom onset. The time of symptom onset was determined from a review of the medical records. Permission to use these clinical neuroimaging data for scientific research was granted by the institutional review board at our medical center.

All examinations were performed on a 1.5-T system (Magnetom Vision; Siemens, Erlangen, Germany) by using circularly polarized clinical head coils and single-shot spin-echo echo-planar pulse sequences with Stejskal-Tanner diffusion gradients (14). Both diffusion-weighted and diffusion-tensor protocols used a 24 × 24-cm field of view, 5-mm section thickness, and 1-mm gap between sections. The diffusion-weighted protocol used a commercial pulse sequence ( $\infty/123$  [repetition time msec/echo time msec];  $b = 1,006$  sec/mm<sup>2</sup>) with a diffusion gradient in only the section-select direction and a 128 × 128-voxel matrix (1.88 × 1.88 × 5.00-mm voxels) that was interpolated to a 256 × 256-pixel matrix. Twenty images were obtained in the entire brain in both transverse and coronal orientations; imag-

ing time for each orientation was 4 seconds.

Unless otherwise stated, the tetrahedral-orthogonal diffusion-tensor protocol and subsequent image processing was performed as described in the Data Acquisition (sequence B) and Data Analysis sections in the article by Shimony et al (11). Briefly, diffusion-tensor data were generated with a single-shot multisection spin-echo echo-planar pulse sequence (3,000/97.4) that used four tetrahedrally oriented diffusion gradients ( $b = 1012.4$  sec/mm<sup>2</sup> with a 22.1 mT/m input gradient strength), three orthogonally oriented diffusion gradients ( $b = 337.5$  sec/mm<sup>2</sup> with the same input strength), and a reference intensity image ( $b = 0$  sec/mm<sup>2</sup>). Fourteen transverse sections were imaged in 35 seconds with a 96 × 128-voxel matrix (2.50 × 1.88 × 5.00-mm voxels with 1-mm gaps) that was interpolated to a 192 × 256-pixel matrix. All images were realigned in two dimensions by using a combination of intra- and cross-modality affine realignment procedures to correct for image displacements and linear stretch and/or shear due to eddy currents (11). Images were postprocessed offline in approximately 45 minutes by using an UltraSPARC 2 Unix workstation (Sun Microsystems, Palo Alto, Calif). A similar tetrahedral-orthogonal diffusion-tensor procedure has been used to investigate water diffusion in the human neonatal brain (15).

Fat-suppressed turbo fluid-attenuated inversion recovery (FLAIR) images (9,999/119/2,309 [repetition time msec/echo time msec/inversion time msec]; echo train length of seven) were obtained in 16 transverse sections of 6-mm thickness with a 1-mm gap between sections (16). Images were acquired in 4 minutes 29 seconds with a 182 × 256-voxel matrix

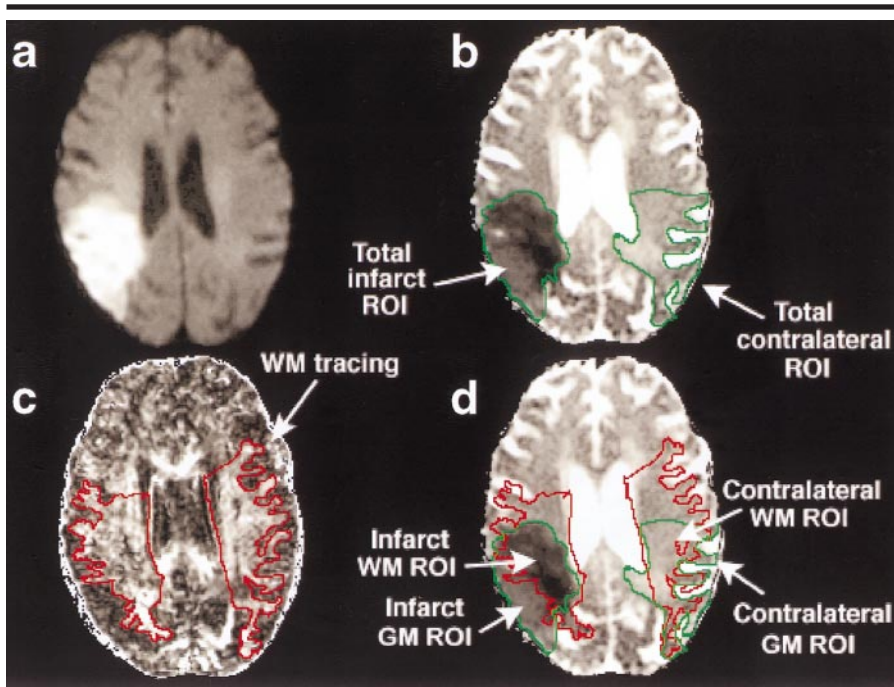


**Figure 1. Patient 10.** Transverse, co-registered, single-shot echo-planar diffusion-tensor images ( $3,000/97.4$ ;  $b = 337.5$  and  $1012.4$  sec/mm<sup>2</sup>) in an 87-year-old woman 3–4 days after right middle cerebral arterial infarct demonstrate the method for the definition of ROIs. *a*, Isotropic diffusion-weighted image (geometric mean of the four tetrahedrally oriented diffusion-weighted images,  $b = 1012.4$  sec/mm<sup>2</sup>) is examined to select the section that traversed the midportion of the lesion. *b*,  $\bar{D}$  image (see Appendix, Eq [A1]) was used to manually trace the outer border of the infarct to define the total infarct ROI. A homologous area is similarly traced in the contralateral hemisphere to define the total contralateral ROI. Both ROI outlines are shown in green. *c*,  $A_v$  image (see Appendix, Eq [A2]) demonstrates white matter (WM) as bright regions of high anisotropy.  $A_v$  images are used to trace the white matter in the vicinity of the infarct and in homologous parts of the contralateral hemisphere (red outlines). Note the correspondence between the gray-white boundary in *c* and the (unmarked) contour in the  $\bar{D}$  image in *b*, which separates the infarct into zones of moderately versus markedly reduced isotropic diffusion. *d*, All four traces are superimposed on the  $\bar{D}$  image. At quantitative analysis, white matter ROIs are defined as regions enclosed by both the red and green outlines, whereas gray matter (GM) ROIs are defined as regions enclosed by the green outline but outside the red outline.

and a  $20 \times 23$ -cm field of view ( $1.10 \times 0.90 \times 6.00$ -mm voxels). The inversion time was optimized to suppress the cerebrospinal fluid signal, and fat was suppressed with radio-frequency pulses. The transverse FLAIR and diffusion-weighted images were oriented along the anterior commissure–to–posterior commissure line. They were, therefore, not necessarily acquired in register with the diffusion-tensor images, which were oriented in the plane transverse to the magnet bore.

### Image Computation

The derivation of the elements of the diffusion tensor  $\mathbf{D}$  from the tetrahedral and perpendicular diffusion measurements is given elsewhere (11). Further details of image computation are also provided in the Appendix. Two useful parameters that can be derived from diffusion-tensor imaging are the directionally

averaged (isotropic) diffusion coefficient ( $\bar{D}$ ) (7) and the diffusion anisotropy measure ( $A_v$ ) (10,17).  $\bar{D}$  represents the component of diffusion that is the same in all directions; that is,  $\bar{D}$  is a general measure of the magnitude of water diffusion averaged over all directions. It is related to the trace of the diffusion tensor and is equivalent to the orthogonally averaged ADC (trace ADC) used previously (7–9).  $A_v$  represents the component of diffusion that varies with spatial direction; that is,  $A_v$  measures the degree to which water diffusion varies with direction. The relatively anisotropic white matter is highlighted on images of  $A_v$ .

Two other types of images were derived from the diffusion-tensor data, namely, isotropic diffusion-weighted images and diffusion-intensity images. Isotropic diffusion-weighted images were computed as the geometric mean of the four tetrahedral diffusion-weighted images. This direc-

tional averaging operation removes the effects of anisotropy while retaining the spin-density and T2 weighting present in unidirectional diffusion-weighted imaging. This procedure is similar to the technique described by Chong et al (18) that is based on the geometric mean of three orthogonal diffusion-weighted images.

The final type of image was the diffusion-intensity image, which represents the component of diffusion-weighted signal intensity that is purely due to isotropic diffusion (19). The diffusion-intensity image is effectively an isotropic diffusion-weighted image on which the spin-density and T2 effects have been removed. As on the  $\bar{D}$  images, the signal intensity on the diffusion-intensity image is solely dependent on isotropic diffusion. The contrast polarity of these diffusion-intensity images is the same as that of the unidirectional and isotropic diffusion-weighted images and opposite to that of the  $\bar{D}$  images. Areas of decreased diffusion appear bright on these diffusion-intensity images, and areas of increased diffusion appear dark.

### Region-of-Interest Analysis

For the measurement of  $\bar{D}$  values, regions of interest (ROIs) were manually traced on a representative transverse image in each patient's data set by using ANALYZE (Mayo Foundation, Rochester, Minn). The representative transverse section was chosen as the one on which the imaging plane passed near the center of the infarct as determined from the isotropic diffusion-weighted image (Fig 1, *a*). A tracing that encompassed the total region of infarction (total infarct ROI) was drawn on the  $\bar{D}$  image (Fig 1, *b*). This  $\bar{D}$  tracing was confirmed to contain all regions of abnormal signal intensity on the corresponding isotropic diffusion-weighted image. A similarly sized region encompassing gray matter and white matter was manually drawn in the contralateral hemisphere (total contralateral ROI). Regions of increased diffusion in periventricular locations (Fig 1, *b*), which were indicative of age-related leukoaraiosis that also appeared as areas of high signal intensity on T2-weighted images, were not excluded from the total contralateral ROI. This was done to assess the baseline  $\bar{D}$  values in noninfarcted brain that were specific to each patient.

$A_v$  images were used to define white matter regions to generate unbiased measurements of gray matter and white matter  $\bar{D}$  values. A tracing that circumscribed the regions of anisotropic diffusion was

drawn on the  $A_\sigma$  image in both hemispheres (Fig 1, c). This  $A_\sigma$  tracing was used to differentiate white matter from gray matter in both the infarct and contralateral ROIs. As illustrated in Figure 1, d, the intersection of the areas enclosed by the  $\bar{D}$  and  $A_\sigma$  tracings was designated as white matter. Areas within the  $\bar{D}$  tracing but outside the  $A_\sigma$  tracing were designated as gray matter. All tracings were drawn by one author (P.M.) and were confirmed to be anatomically accurate by a board-certified radiologist with a certificate of added qualification in neuroradiology (M.M.B.) and a second board-certified radiologist (T.E.C.).

This procedure typically generated one to four closed regions of gray matter in each hemisphere in each patient. Multiple gray matter regions occurred more commonly on the contralateral side (Fig 1, d). In patients with multiple regions, the gray matter region on each side with the largest area and the least-visible partial-volume averaging with adjacent cerebrospinal fluid was chosen as the infarct or contralateral gray matter ROI for further analysis. In white matter, this procedure typically yielded only one closed region on each side. In the few cases with more than one closed region of white matter, the region with the largest area was selected as the infarct or contralateral white matter ROI for further analysis. No partial-volume effects with cerebrospinal fluid were noted in the white matter regions.

The mean and SD of the  $\bar{D}$  pixel values were computed in each ROI in each of the 12 patients. The mean  $\bar{D}$  values in the ROIs were compared across patients with a paired two-population two-tailed Student *t* test by using Origin 4.1 (Microcal Software, Northampton, Mass). Figures were prepared by using Photoshop 4.0 for Windows (Adobe Systems, San Jose, Calif) to create montages; to adjust size, brightness, and contrast; and to remove background noise outside of the brain. Brain images were not edited except for the placement of markers to indicate findings of special interest.

## RESULTS

Isotropic diffusion was found to be less in infarcted white matter than in infarcted gray matter in all 12 patients. This difference was apparent as gray-white contrast in the infarct on both  $\bar{D}$  and diffusion-intensity images (Fig 2). However, the signal intensity in gray matter was greater than that of white matter in the infarct on diffusion- and T2-weighted images.

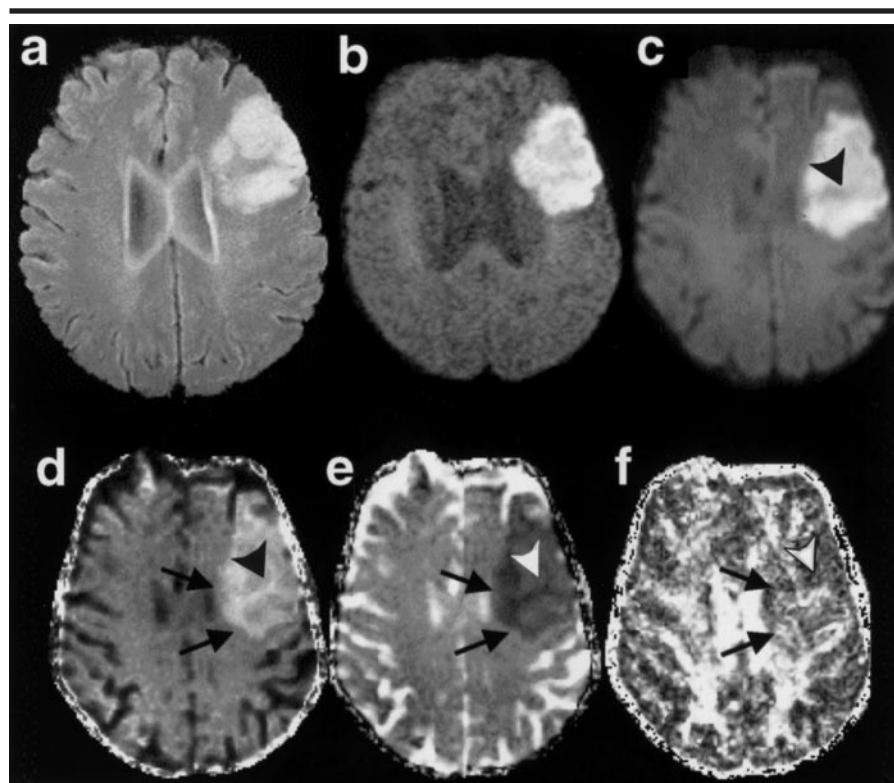


**Figure 2. Patient 1.** Transverse images obtained in a 71-year-old woman 46 hours after left middle cerebral arterial infarction show differences between gray matter and white matter diffusion. Sections in *a* and *b* correspond to sections in *c-f* only approximately. *a*, FLAIR image (9,999/119/2,309). *b*, Unidirectional diffusion-weighted image ( $\infty/123$ ;  $b = 1,006$  sec/mm<sup>2</sup>). Note the prominent increase in signal intensity in the infarcted cortical gray matter. *c-f*, Single-shot echo-planar diffusion-tensor images (3,000/97.4;  $b = 337.5$  and 1,012.4 sec/mm<sup>2</sup>). Images and superimposed markers are co-registered. *c*, Isotropic diffusion-weighted image. *d*, Diffusion-intensity image (see Appendix, Eq [A4]). The diffusion-intensity image is equivalent to the isotropic diffusion-weighted image after the removal of spin-density, T1, and T2 weighting. *e*,  $\bar{D}$  image. *f*,  $A_\sigma$  image. The bright area of abnormal signal intensity in the subcortical white matter (arrowhead in *c-f*) and deep white matter (medial border of corona radiata [arrows in *d-f*]) is in register with the zone of the greatest decrease in  $\bar{D}$  in *e*. Image in *f* confirms that these areas of markedly reduced  $\bar{D}$  correspond to white matter. The highly anisotropic structure medial to the corona radiata is the body of the corpus callosum, as confirmed at imaging of the lower adjacent sections (not shown).

(The preponderance of gray matter in the areas of abnormal signal intensity on T2-weighted images can help explain this discrepancy between the findings on diffusion-weighted and diffusion-intensity images in acute stroke [see Discussion]).

In four of the 12 patients, white matter regions had abnormal diffusion on  $\bar{D}$  and diffusion-intensity images but appeared relatively spared on diffusion- and T2-weighted images (Fig 3). On diffusion-weighted images, the areas of apparent white matter sparing were located adjacent to areas of gray matter with abnormally high signal intensity.

In all 12 patients, the  $\bar{D}$  and diffusion-intensity images showed lesion heterogeneity that was characterized by two distinct levels of diffusion reduction termed moderate and marked (Figs 1b, 2d, 2e, 3d,

3e, 4d, 4e). In all patients, markedly reduced diffusion occurred exclusively in white matter, while moderately reduced diffusion occurred exclusively in gray matter. This assignment was based on two observations. First, in all 12 patients, the regions of infarct that demonstrated anisotropic diffusion also had markedly reduced  $\bar{D}$  values (Figs 1c, 1d, 2e, 2f, 3e, 3f, 4e, 4f). This means that all regions of infarcted white matter with detectable anisotropy had markedly reduced diffusion. Second, and in converse, the entire region of markedly reduced  $\bar{D}$  values also demonstrated anisotropic diffusion in 10 of the 12 patients (Figs 1c, 1d, 2e, 2f, 3e, 3f).

In the other two patients (who underwent imaging 3–5 days after stroke onset [Patients 2 and 5 in Tables 1, 2]), some regions with markedly reduced  $\bar{D}$  values

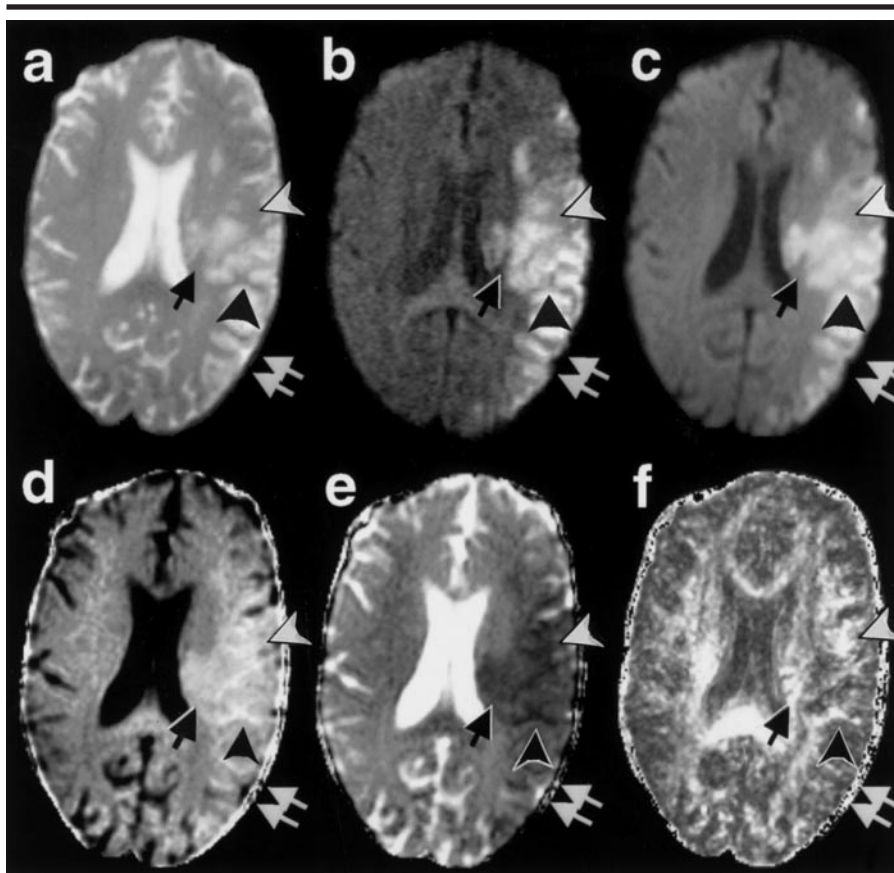


**Figure 3. Patient 8.** Transverse images obtained in a 61-year-old man 3–4 days after left middle cerebral arterial infarct show findings in early subacute stroke with maintained anisotropy. *a*, T2-weighted echo-planar ( $b = 0 \text{ sec/mm}^2$ ); *b*, unidirectional; and *c*, isotropic diffusion-weighted images show prominent areas of abnormal signal intensity in the cortical gray matter with relative sparing of the subcortical white matter (white arrows, arrowheads) and internal capsule (black arrow). *d*, Diffusion-intensity and *e*,  $\bar{D}$  images demonstrate that the apparently spared areas in *a*–*c* exhibit a greater degree of diffusion reduction (bright in *d*, dark in *e*) and are identifiable as white matter on the  $A_{\sigma}$  image in *f*. Images and superimposed markers in *a* and *c*–*f* are co-registered.

did not have visible anisotropy. This is compatible with a loss of white matter anisotropy in the later stages of stroke evolution (20–22). However, in these two patients, regions with markedly reduced  $\bar{D}$  values had a morphology that was characteristic of white matter (Fig 4e, 4f). Thus, all regions with markedly reduced diffusion were white matter.

Table 2 lists the  $\bar{D}$  values in all 12 patients. The mean  $\bar{D}$  value in the total infarct ROI was  $(0.54 \pm 0.09) \times 10^{-3} \text{ mm}^2/\text{sec}$  and included both white matter and gray matter. This value was significantly less than the mean  $\bar{D}$  value in the total contralateral ROI, which was  $(0.89 \pm 0.07) \times 10^{-3} \text{ mm}^2/\text{sec}$  ( $P < .001$ ). The percent reduction of  $\bar{D}$  values in the total infarct ROI relative to that in the total contralateral ROI was  $39\% \pm 10$ . Both gray matter and white matter exhibited decreased  $\bar{D}$  values in the infarct com-

pared with the values in the contralateral hemisphere. The percent reduction of  $\bar{D}$  values in infarcted gray matter averaged across all 12 patients was  $31\% \pm 7$ , relative to that of contralateral hemisphere. In infarcted white matter, the percent reduction of  $\bar{D}$  values was  $46\% \pm 12$ . This difference between white matter and gray matter was significant ( $P < .001$ ).

In the infarcted regions,  $\bar{D}$  values in white matter were less than those in gray matter in every patient. This is illustrated in Figure 5, which shows that the  $\bar{D}$  values in all infarct ROIs are above the line of identity, that is, the line that indicates equal gray matter and white matter diffusion. The mean  $\bar{D}$  value in affected white matter across all patients was  $(0.46 \pm 0.10) \times 10^{-3} \text{ mm}^2/\text{sec}$  and was significantly less ( $P < .001$ ) than the mean  $\bar{D}$  value in affected gray matter, which was  $(0.61 \pm 0.06) \times 10^{-3} \text{ mm}^2/\text{sec}$ .

In addition, differences between  $\bar{D}$  values in gray matter and white matter tended to be greater at lower overall values of  $\bar{D}$ . (Note the divergence of the infarct regression line from the line of identity in Figure 5.) The slope of the regression line that best fit the infarct data was 0.51 (Fig 5), which was significantly different from the unit slope ( $P < .01$ ). In contrast, contralateral hemisphere data in the 12 patients was not significantly different; the mean value of  $\bar{D}$  was  $(0.86 \pm 0.08) \times 10^{-3} \text{ mm}^2/\text{sec}$  in white matter and  $(0.88 \pm 0.08) \times 10^{-3} \text{ mm}^2/\text{sec}$  in gray matter ( $P > .05$ ).

Subgroup analysis of the six patients who underwent imaging within 72 hours of stroke onset (<3-days group, Table 1) revealed mean  $\bar{D}$  values of  $(0.42 \pm 0.08) \times 10^{-3} \text{ mm}^2/\text{sec}$  in affected white matter and  $(0.59 \pm 0.07) \times 10^{-3} \text{ mm}^2/\text{sec}$  in affected gray matter ( $P < .001$ ). In the six patients who underwent imaging 3–5 days after infarction, the difference in white matter and gray matter diffusion remained significant ( $P < .01$ );  $\bar{D}$  values were  $(0.51 \pm 0.11) \times 10^{-3} \text{ mm}^2/\text{sec}$  and  $(0.62 \pm 0.06) \times 10^{-3} \text{ mm}^2/\text{sec}$ , respectively. The difference between white matter and gray matter in the percentage reduction in  $\bar{D}$  values was significant in both the <3-days group ( $P < .001$ ) and the 3–5-days group ( $P < .05$ ), although the percentage decrease in  $\bar{D}$  was less in the latter case.

The reduction in the  $\bar{D}$  values in white matter tended to be greater in the <3-days group ( $53\% \pm 9$  decrease) than in the 3–5-days group ( $39\% \pm 12$  decrease), but this difference was not statistically significant ( $P > .05$ ). The percent reduction in gray matter  $\bar{D}$  values was similar in the <3-days group ( $33\% \pm 7$  decrease) and 3–5-days group ( $28\% \pm 7$  decrease,  $P > .05$ ). The mean percentage reduction in  $\bar{D}$  values in the total infarct ROI relative to that of the total contralateral ROI was greater in the <3-days group ( $45\% \pm 8$ ) than in the 3–5-days group ( $34\% \pm 10$ ), but this difference was not statistically significant ( $P > .05$ ) with these sample sizes.

## DISCUSSION

Previous MR imaging investigations (7–9) of acute cerebral ischemia have not revealed appreciable differences between gray matter and white matter ADCs in infarcted regions relative to those in regions of unaffected brain. However, the orthogonal diffusion encoding used in those studies did not have a signal-to-

noise ratio as high as that of the diffusion-tensor method used herein (10,11). Furthermore, in those previous studies, quantitative measures of isotropic diffusion in gray matter and white matter were not compared, and information about anisotropy was not used to distinguish white matter from gray matter. In addition, we used precise image realignment that was tailored to minimize misregistration that could otherwise have degraded the spatial resolution of gray matter and white matter regions (11).

In one diffusion-tensor study of hyperacute and early acute stroke, Sorensen et al (23) reported no statistically significant difference in isotropic diffusion in ischemic gray matter and white matter. Their result raises the possibility that the difference between gray matter and white matter diffusion reported herein might not be present in the initial hyperacute phase of stroke. However, their study was not specifically designed to investigate diffusion differences in gray matter and white matter in individual patients. Many of their patients had infarcts that were isolated to only gray or white matter.

In the present study, we examined patients with infarcts that encompassed confluent regions of both gray matter and white matter. In this design, each patient served as his or her own control subject in terms of the relative magnitude of changes in gray matter and white matter diffusion in the infarcted territory compared with the changes in the uninvolved contralateral hemisphere. Therefore, further research is needed to resolve whether the differences in gray matter and white matter diffusion established herein in acute to early subacute stroke are also detectable in the clinically important hyperacute stage. Follow-up serial imaging of these patients during the acute and subacute stages would also be helpful in the definition of the time course of stroke-related diffusion alterations in white matter versus gray matter.

The 39% decrease in  $\bar{D}$  values in the first 5 days after infarction that was found in this investigation agrees with the 41.7% decrease in ADC values in the first 4 days after stroke onset that was determined in a large study of 157 patients (13). The accuracy of the  $\bar{D}$  values in the present study is further supported by measurements obtained in regions contralateral to the infarct; these measurements are well within the range reported both in healthy volunteers (12,24) and in uninvolved brain regions in stroke patients (9,25). We also found no statistically significant difference in  $\bar{D}$  values in contra-

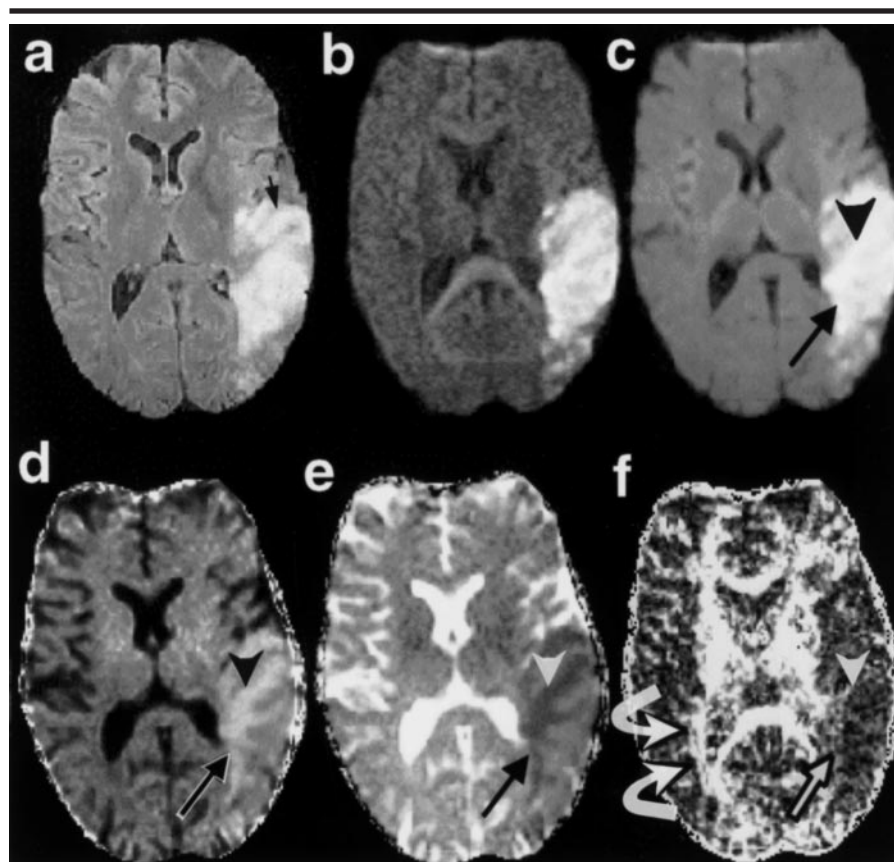


**Figure 4. Patient 5.** Transverse images obtained in a 41-year-old woman 5 days after left middle cerebral arterial infarct show findings in early subacute stroke with markedly reduced anisotropy. *a*, FLAIR image (9,999/119/2,309) shows abnormal signal intensity predominantly in the gray matter in the posterior insular region (arrow) and shows mixed areas of abnormal signal intensity in the gray matter and white matter in the posterior temporal lobe. *b*, Unidirectional and *c*, isotropic diffusion-weighted images demonstrate heterogeneous areas of abnormal signal intensity in the infarct, with subtle prominence of white matter such as the optic radiations (straight arrow in *c-f*). *d*, Diffusion-intensity and *e*,  $\bar{D}$  images exhibit a contrast pattern similar to that in Figures 2 and 3. Regions of markedly reduced diffusion (bright in *d*, dark in *e*) have the morphology of white matter, including the optic radiations (straight arrow). *f*,  $A_{\sigma}$  image shows severe loss of anisotropy in the infarct, as seen in the optic radiations, compared with the contralateral side (curved arrows). Regions of residual anisotropy (arrowhead in *c-f*) were used to trace the white matter at ROI analysis. Images in *c-f* and superimposed markers are co-registered.

lateral gray matter and white matter. These findings agree with those of quantitative diffusion MR imaging studies in healthy adults (12,24,26).

The larger values of  $\bar{D}$  in infarcted gray matter relative to those in infarcted white matter cannot be explained by the effect of partial-volume averaging with cerebrospinal fluid. These differences persisted even after normalization with the data obtained from the contralateral side, where partial-volume averaging of cortex with cerebrospinal fluid is more likely. Partial-volume averaging with cerebrospinal fluid was less consequential in the infarct ROIs than in the contralateral ROIs because of the sulcal effacement that is characteristic of acute and early subacute stroke. Furthermore, no statisti-

cally significant difference in  $\bar{D}$  values was found in white matter and gray matter ROIs in the contralateral hemisphere (Table 2). This finding suggests that cerebrospinal fluid averaging in gray matter was effectively minimized in the contralateral gray matter ROIs, as well.

Information about anisotropy, obtained by using the  $A_{\sigma}$  measure, was the sole criterion that was used in the differentiation of white matter and gray matter in this study, since white matter has much greater anisotropy than does gray matter (11,26,27). However, white matter anisotropy decreases in areas in which infarction is evolving (20–22). A small decline in anisotropy has also been reported in acute stroke (23). In our study, enough residual anisotropy remained to allow

**TABLE 2**  
 **$\bar{D}$  Values Measured in Acute to Early Subacute Middle Cerebral Arterial Infarcts and in Contralateral Hemispheres**

Patient No.	Infarct ROI ( $10^{-3}$ mm <sup>2</sup> /sec)			Contralateral ROI ( $10^{-3}$ mm <sup>2</sup> /sec)			Decrease* (%)		
	White Matter	Gray Matter	Total	White Matter	Gray Matter	Total	White Matter	Gray Matter	Total
1	0.50	0.60	0.55	0.91	0.85	0.90	45	29	39
2	0.43	0.56	0.55	0.68	0.77	0.72	37	26	24
3	0.47	0.67	0.56	0.89	0.93	0.93	47	28	40
4	0.41	0.56	0.51	0.77	0.79	0.85	46	30	41
5	0.54	0.61	0.62	0.96	0.98	0.97	43	37	36
6	0.62	0.71	0.68	0.89	0.99	0.95	29	28	28
7	0.27	0.47	0.35	0.84	0.86	0.86	69	45	60
8	0.61	0.66	0.66	0.80	0.79	0.87	23	16	25
9	0.46	0.64	0.53	0.93	0.96	0.98	50	33	46
10	0.40	0.60	0.48	0.91	0.89	0.95	56	33	49
11	0.39	0.62	0.53	0.88	0.86	0.90	56	28	41
12	0.43	0.56	0.51	0.85	0.84	0.85	50	33	41
Mean $\pm$ SD	0.46 $\pm$ 0.10	0.61 $\pm$ 0.06	0.54 $\pm$ 0.09	0.86 $\pm$ 0.08	0.88 $\pm$ 0.08	0.89 $\pm$ 0.07	46 $\pm$ 12	31 $\pm$ 7	39 $\pm$ 10

\* Percent decrease in mean  $\bar{D}$  of the infarct ROI relative to the corresponding ROI in the contralateral hemisphere.

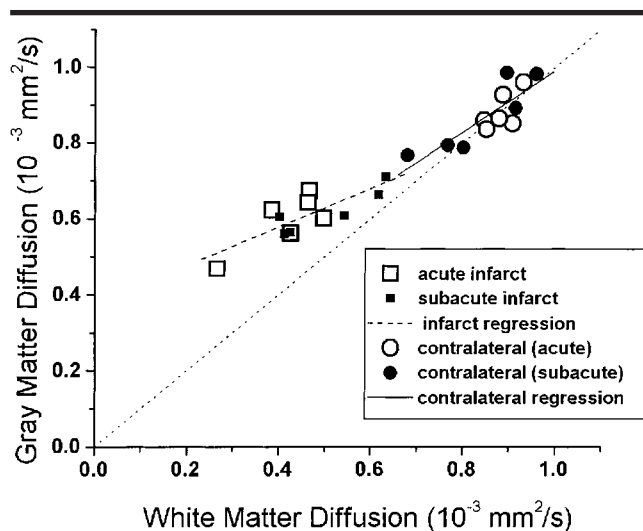


**Figure 5.** Plot shows the regression analysis of the  $\bar{D}$  values in gray matter versus white matter. ROIs in all 12 patients are represented. Line of identity (dotted line) corresponds to equal white matter  $\bar{D}$  and gray matter  $\bar{D}$ . Line of regression for infarct data has a slope of  $0.51 \pm 0.12$ , which is significantly different from unity ( $t_{10} = -4.24, P < .01$ ). Regression line for the data in contralateral ROIs has a slope of  $0.81 \pm 0.17$ , which is not significantly different from unity ( $t_{10} = -1.13, P > .05$ ). Note the following: First, all data from infarct ROIs lie above the line of identity, thus demonstrating the highly consistent gray-white contrast in the infarct. Second, the infarct regression line diverges from the line of identity as the reduction in  $\bar{D}$  becomes more severe. Third, gray-white  $\bar{D}$  contrast tends to be more pronounced in infarcts less than 3 days old (open squares) than in those 3–5 days old (solid squares). Last, infarct and contralateral data do not overlap, which suggests that the quantitative measurement of  $\bar{D}$  is a highly sensitive test for the detection of acute and early subacute infarcts.

adequate identification of infarcted white matter in 10 of 12 patients (Figs 1–3). In six of the 12 patients, the infarcted region was sufficiently distorted from mass effect so that areas of markedly decreased diffusion could not be confidently identified as white matter on  $\bar{D}$  images alone

without correlation with  $A_{\sigma}$  images (Figs 1, 3). Correlation of the contrast patterns on  $\bar{D}$  and  $A_{\sigma}$  images may be important for the differentiation of diffusion contrast due to tissue type (ie, gray vs white matter) from diffusion contrast due to heterogeneity of the ischemic process.

Two of the 12 patients had severe reductions in anisotropy in the infarct, and both reductions involved early subacute stroke. Despite these findings, only regions of residual anisotropy were used to objectively measure  $\bar{D}$  values in white matter. Nevertheless, the  $\bar{D}$  images demonstrated regions of markedly reduced diffusion that extended beyond the regions of residual anisotropy; the regions had the morphology of white matter (temporal lobe in Fig 4). In these two patients, the use of  $A_{\sigma}$  values to segment white matter likely resulted in the inclusion of areas of white matter within the zone that was deemed to be gray matter.

However, this averaging of white matter with gray matter reduces apparent differences between the two tissue types rather than causes artifactual differences where none exists. An exception is if there is preferential loss of anisotropy in regions where  $\bar{D}$  values are not substantially reduced (eg, selective loss of anisotropy in the periphery of the lesion with a more severe reduction in  $\bar{D}$  values in the center of the lesion where anisotropy is preserved). Such a scenario is unlikely given the pattern of anisotropy loss in Figure 4, *f* and the relative uniformity of the reduction in  $\bar{D}$  values in white matter in Figures 1–4. However, additional experience with cases of marked loss of anisotropy in subacute stroke is needed for a full evaluation of this possibility.

Diffusion-weighted imaging within the first 48 hours of stroke typically shows greater increases in signal intensity in gray matter than in white matter (Figs 2*b*, 3*b*); this finding is similar to the contrast pattern on T2-weighted images (Figs 2*a*, 3*a*). Traditionally, gray matter has been

considered to be more vulnerable than white matter to the early effects of ischemia (28); this consideration would appear to be corroborated by the findings of diffusion-weighted imaging.

After the initial 48 hours, the area of abnormal signal intensity on diffusion-weighted images typically becomes more homogeneous. It extends throughout the region of infarction with little or no gray-white contrast (Fig 1, *a* and posterior temporal lobe in Fig 4, *b*). This contrast pattern can also be observed on T2-weighted images (posterior temporal lobe in Fig 4, *a*). The progression of the area of abnormal signal intensity on diffusion-weighted images over time—from a predominant distribution in gray matter in acute infarcts to a more uniform involvement of both gray matter and white matter in subacute infarcts—was noted in the earliest diffusion-weighted studies of stroke (eg, fig 2 in reference 2).

However, these diffusion-weighted imaging findings should not necessarily be interpreted as an indication that the underlying diffusion abnormality is greater in gray matter than in white matter. In fact, the data herein demonstrate that the diffusion abnormality is greater in infarcted white matter. The predominant involvement of gray matter in acute stroke on diffusion-weighted images with more uniform involvement of gray matter and white matter in early subacute stroke results from multiplicative signal effects from elevated T2-weighted signal with diffusion-weighted imaging (see Appendix, Eq [A5]).

The areas of high signal intensity on T2-weighted FLAIR images are predominantly distributed in the gray matter in acute infarcts (Fig 2, *a*) and progress to a more homogenous involvement of gray matter and white matter in the early subacute phase (Fig 4, *a*). This evolution of signal intensity on T2-weighted images is similar to that on diffusion-weighted images and has been also attributed to the greater vulnerability of gray matter to early ischemia (29,30).

FLAIR images are useful in the determination of the relative contribution of T2-weighted effects to diffusion-weighted imaging because FLAIR and diffusion-weighted imaging are both T2-weighted and cerebrospinal fluid-suppressed, yet FLAIR imaging is insensitive to diffusion (31). Hence, areas of increased signal intensity on FLAIR images contribute to contrast with diffusion-weighted imaging. These signal effects in gray matter with T2-weighted imaging (Fig 2, *a*) were especially pronounced on unidirectional

diffusion-weighted images (Fig 2, *b*) compared with isotropic diffusion-weighted imaging (Fig 2, *c*). This is because the longer echo time of the unidirectional diffusion-weighted sequence (123.0 vs 97.4 msec) more closely matches the characteristic range of T2 values in the infarct.

Diffusion-weighted imaging has been shown to have better sensitivity, specificity, and accuracy in the detection of acute stroke than does trace ADC imaging (18). Those authors attribute this to T2-weighted effects with diffusion-weighted imaging, which trace ADC images lack. Their results agree with our findings, as the infarcts in Figures 1–4 were more conspicuous on diffusion-weighted images than on diffusion-intensity images, which also lack T2 weighting. We refer to this phenomenon as cooperative contrast between T2 and diffusion (32), which amplifies the contrast between ischemic and normal gray matter in diffusion-weighted imaging. Thus, diffusion-intensity imaging may be expected to be less sensitive than diffusion-weighted imaging for the detection of small focal cortical infarcts when changes in T2-weighted signal are present.

However, our comparison of diffusion-weighted and diffusion-intensity imaging indicate that diffusion-weighted imaging may cause underestimation of the magnitude and spatial extent of white matter involvement in stroke. In all 12 patients, diffusion-intensity images demonstrated more severe diffusion changes in white matter compared with those in gray matter, whereas areas of abnormal signal intensity on diffusion-weighted images were equal in the two tissues or were greater in gray matter. In four of the 12 patients, diffusion-intensity images showed regions of white matter involvement that appeared relatively spared at diffusion-weighted imaging (Fig 3). The lower sensitivity of diffusion-weighted imaging to white matter ischemia may be secondary to less contrast amplification from T2 effects, which are delayed in white matter compared with gray matter. Consequently, subtle changes in white matter on diffusion-weighted images may not be visible adjacent to the large changes in signal intensity in the surrounding gray matter.

Differences in gray matter and white matter diffusion in stroke could be due to variability between these two tissue types at any stage in the process that leads from ischemia to altered diffusion. Specifically, the observed diffusion contrast in gray matter and white matter could be caused by differences in (*a*) the mismatch be-

tween blood supply and metabolic demand (ischemia), (*b*) the type and/or severity of the histopathologic response to ischemic injury (vulnerability), or (*c*) the mechanisms by which histopathologic changes lead to altered diffusion. Findings from positron emission tomographic studies suggest that the flow-metabolism mismatch is similar in gray matter and white matter in middle cerebral arterial infarcts. (For example, see the uniformity of oxygen extraction fraction images in figure 1 in the article by Carpenter et al [33]).

Regarding the histopathologic response, gray matter has been traditionally considered to be more vulnerable than white matter to early ischemia (28). However, more recent findings in experimental models of stroke have demonstrated that ischemic damage to white matter occurs earlier and with greater severity than previously appreciated. In two studies, one conducted in rats within 24 hours of middle cerebral arterial occlusion (34) and the other conducted in cats within 3 hours of middle cerebral arterial occlusion (35), investigators documented histopathologic changes in affected white matter as early as 30 minutes after the onset of ischemia. Astrocytic swelling secondary to cytotoxic edema occurred in both white matter and gray matter, and white matter also displayed hydropic swelling of oligodendroglial cell bodies. Immunocytochemical experiments in which rat models of middle cerebral arterial stroke were used revealed pathophysiologic axonal changes in myelinated white matter within 4–6 hours after arterial occlusion (36,37) that are similar to those that resulted from traumatic diffuse axonal injury (37). Findings from these investigations highlight the vulnerability of white matter to even short periods of ischemia.

Regarding the histopathologic-biophysical diffusion mechanisms, intracellular accumulation of water and enlargement of the periaxonal space were found in myelinated fiber tracts in animal models (34,35), with differences in the dependence of ischemic gray matter and white matter diffusion on total water accumulation (35). Findings from these studies suggest that intra- and extracellular accumulation of fluid and resultant changes in diffusion might differ significantly in white matter and gray matter. Finally, additional histopathologic-biophysical mechanisms of diffusion reduction that do not exist in gray matter might occur in white matter; these mechanisms include reduced bulk water motion from cytoskel-

etal breakdown and disruption of fast axonal transport (36,37).

If the results from previous animal experiments can be generalized to humans, they may provide a pathophysiologic basis for the gray-white diffusion contrast found in this investigation. The rapid onset of the changes in white matter in these animal studies is also consistent with our findings, as gray-white diffusion contrast was observed at all of the time intervals after stroke onset that were studied, including the earliest (17 hours). These results suggest that this gray-white diffusion contrast represents a fundamental difference in the diffusion response of gray matter and white matter to ischemia and that these two tissues should be separately evaluated in studies of the quantitative assessment of neuroprotective therapy (38–40) or infarct heterogeneity (25,41).

In summary, diffusion-tensor imaging of acute and early subacute middle cerebral arterial infarcts demonstrates more severe reductions in isotropic diffusion in white matter than in gray matter, whereas diffusion-weighted imaging appears to cause underestimation of the magnitude and spatial extent of white matter involvement. The observed disparity in diffusion in gray matter and white matter at diffusion-tensor imaging increased with increasing overall magnitude of diffusion reduction. The discrepancy between diffusion-weighted and diffusion-tensor images was due to areas of increased signal intensity in the infarct on T2-weighted images; this increase appeared earlier and more often in gray matter than in white matter.

Diffusion-tensor imaging provides a full complement of isotropic diffusion, anisotropy, and diffusion-weighted images for the assessment of acute stroke in both white matter and gray matter. The images and measurements of diffusion in gray matter and white matter presented herein may be relevant to the interpretation of diffusion-weighted images, clinical treatment and rehabilitation of stroke patients, evaluation of neuroprotective therapies in acute stroke, and basic scientific studies of the pathophysiologic mechanisms of stroke and infarct heterogeneity. Further investigation of diffusion-tensor imaging is needed in the hyperacute phase of stroke, when results may affect the early clinical treatment of patients.

## APPENDIX

In each pixel, the entire diffusion tensor was fit to the eight log-intensities that

corresponded to the seven diffusion encoding directions and the reference T2-weighted intensity image ( $b = 0 \text{ sec/mm}^2$ ) (11). From this estimated tensor  $\mathbf{D}$ , the directionally averaged diffusivity  $\bar{D}$  value (an invariant measure of isotropic diffusion with units of square millimeter per second) was calculated as the arithmetic mean of the three diagonal elements of  $\mathbf{D}$  as follows (7):

$$\bar{D} = \frac{1}{3} (D_{xx} + D_{yy} + D_{zz}). \quad (\text{A1})$$

That is, the  $\bar{D}$  value is one-third the trace of  $\mathbf{D}$ , where the trace is the sum of the eigenvalues of  $\mathbf{D}$ .  $\bar{D}$  has also been referred to as  $D_{av}$  (9) or trace ADC in studies in which the diffusion coefficient was averaged over different encoding directions to remove the effects of anisotropy.  $\bar{D}$  is invariant to the coordinate system used to measure  $\mathbf{D}$  and, thus, is not affected by the orientation of the head or the direction of white matter fibers.

The dimensionless absolute measure of anisotropy  $A_\sigma$  was computed on a pixel-by-pixel basis from the elements of  $\mathbf{D}$  as follows (10):

$$A_\sigma = \frac{1}{\sqrt{6} \bar{D}} \times \sqrt{\sum_{i=x,y,z} (D_{ii} - \bar{D})^2 + 2(D_{xy}^2 + D_{xz}^2 + D_{yz}^2)}, \quad (\text{A2})$$

where the  $A_\sigma$  value is equivalent to the coefficient of variation of the eigenvalues of  $\mathbf{D}$  divided by the square root of 2 (10). It is directly proportional to the relative anisotropy defined by Basser and Pierpaoli (17), with a scaling factor of the square root of  $\frac{1}{2}$ , which places the value of  $A_\sigma$  on an absolute scale from 0 (no anisotropy) to 1 (complete anisotropy). Like  $\bar{D}$ ,  $A_\sigma$  is invariant to the measurement coordinate system used to define the elements of  $\mathbf{D}$ .

With echo times that are much shorter than T1 relaxation times, the intensity  $I_{DWI}$  of the isotropic diffusion-weighted image is related to diffusion, T1 weighting, spin density, and T2 weighting as follows:

$$I_{DWI} \propto \rho e^{-b\bar{D}} e^{-TE/T2} (1 - e^{-(TR-TE)/T1}), \quad (\text{A3})$$

where  $\rho$  is the scalar spin density in the voxel;  $b$  is the diffusion-weighting factor; TE is the echo time; TR is the repetition time; and T1 and T2 are the longitudinal and transverse relaxation times, respectively. In single-shot echo-planar imaging techniques in which only one encoding direction is acquired per pulse sequence acquisition, the effective repetition time

is infinite; hence, there is no T1 weighting.

The diffusion-intensity image  $I_{DI}$  was computed by the method introduced by Sorensen et al (19) as follows:

$$I_{DI} \propto e^{-b\bar{D}}, \quad (\text{A4})$$

where  $b = 1,000 \text{ sec/mm}^2$ .

The intensity of the isotropic diffusion-weighted image  $I_{DWI}$  can thus be expressed in terms of the intensities of the diffusion-intensity image  $I_{DI}$  and the reference T2-weighted-intensity image  $I_{T2WI}$  as follows:

$$I_{DWI} = I_{DI} \cdot I_{T2WI}, \quad (\text{A5})$$

where the T2-weighted intensity image is acquired with  $b = 0 \text{ sec/mm}^2$  and has the same spin-density, T1, and T2 effects as those of the isotropic diffusion-weighted images. Equation (A5) defines the multiplicative interaction between diffusion and T2-weighted signals.

## References

1. Hacke W, Kaste M, Sieschi C, et al. Random double-blind placebo-controlled trial of thrombolytic treatment with intravenous Alteplase in acute ischemic stroke (ECASS II). *Lancet* 1998; 352:1245–1251.
2. Warach S, Chien D, Li W, Ronthal M, Edelman RR. Fast magnetic resonance diffusion-weighted imaging of acute human stroke. *Neurology* 1992; 42:1717–1723.
3. Warach S, Gaa J, Siewert B, Wielopolski P, Edelman RR. Acute human stroke studied by whole brain diffusion-weighted MRI. *Ann Neurol* 1995; 37:231–241.
4. Sorensen AG, Buonanno FS, Gonzalez RG, et al. Hyperacute stroke: evaluation with combined multisection diffusion-weighted and hemodynamically weighted echoplanar imaging. *Radiology* 1996; 199:391–401.
5. Beauchamp NJ Jr, Ulug AM, Passe TJ, van Zijl PC. MR diffusion imaging in stroke: review and controversies. *RadioGraphics* 1998; 18:1269–1283.
6. Warach S, Boska M, Welch KM. Pitfalls and potential of clinical diffusion-weighted imaging in acute stroke. *Stroke* 1997; 28:481–482.
7. van Gelderen P, de Vleeschouwer MH, DesPres D, Pekar J, van Zijl PC, Moonen CT. Water diffusion and acute stroke. *Magn Reson Med* 1994; 31:154–163.
8. Mori S, van Zijl PC. Single-scan magnetic resonance imaging of the trace of the diffusion tensor. *Magn Reson Med* 1995; 33:41–52.
9. Ulug AM, Beauchamp NJ Jr, Bryan RN, van Zijl PC. Absolute quantitation of diffusion constants in human stroke. *Stroke* 1997; 28:483–490.
10. Conturo TE, McKinsty RC, Akbudak E, Robinson BH. Encoding of anisotropic diffusion with tetrahedral gradients: a general mathematical diffusion formalism and experimental results. *Magn Reson Med* 1996; 35:399–412.
11. Shimony JS, McKinsty RC, Akbudak E, et al. Quantitative diffusion-tensor anisotropy

- ropy brain MR imaging: normative human data and anatomic analysis. *Radiology* 1999; 212:770-784.
12. Shimony JS, McKinstry RC, Akbudak E, Snyder AZ, Aronovitz JA, Conturo TE. Cerebral diffusion tensor imaging: normative data, signal-to-noise measurements, and anatomical findings (abstr). In: Proceedings of the Fifth Meeting of the International Society for Magnetic Resonance in Medicine. Berkeley, Calif: International Society for Magnetic Resonance in Medicine, 1997; 225.
  13. Schlaug G, Siewert B, Benfield A, Edelman RR, Warach S. Time course of the apparent diffusion coefficient (ADC) abnormality in human stroke. *Neurology* 1997; 49:113-119.
  14. Turner R, Le Bihan D, Chesnick AS. Echoplanar imaging of diffusion and perfusion. *Magn Reson Med* 1991; 19:247-253.
  15. Neil JJ, Shiran SI, McKinstry RC, et al. Normal brain in human newborns: apparent diffusion coefficient and diffusion anisotropy measured by using diffusion tensor MR imaging. *Radiology* 1998; 209:57-66.
  16. Hajnal JV, Bryant DJ, Kasuboski L, et al. Use of fluid-attenuated inversion recovery (FLAIR) pulse sequences in MRI of the brain. *J Comput Assist Tomogr* 1992; 16:841-844.
  17. Bassner PJ, Pierpaoli C. Microstructural and physiological features of tissues elucidated by quantitative-diffusion-tensor MRI. *J Magn Reson B* 1996; 111:209-219.
  18. Chong J, Lu D, Aragao F, et al. Diffusion-weighted MR of acute cerebral infarction: comparison of data processing methods. *Am J Neuroradiol* 1998; 19:1733-1739.
  19. Sorensen AG, Weisskopf RM, Reese TR, Rosen BR. Optimization of diffusion-weighted MR imaging for evaluation of acute stroke (abstr). In: Proceedings of the Third Meeting of the International Society for Magnetic Resonance in Medicine. Berkeley, Calif: International Society for Magnetic Resonance in Medicine, 1995; 1383.
  20. Pierpaoli C, Penix L, De Graba T, Bassner PJ, Di Chiro G. Identification of fiber degeneration and organized gliosis in stroke patients by diffusion tensor MRI (abstr). In: Proceedings of the Fourth Meeting of the International Society for Magnetic Resonance in Medicine. Berkeley, Calif: International Society for Magnetic Resonance in Medicine, 1996; 563.
  21. Carano RAD, Li F, Irie K, Fisher M, Sotak CH. The temporal evolution of diffusion anisotropy in the ischemic rat brain (abstr). In: Proceedings of the Sixth Meeting of the International Society for Magnetic Resonance in Medicine. Berkeley, Calif: International Society for Magnetic Resonance in Medicine, 1998; 530.
  22. Zelaya F, Flood N, Chalk J, Wang D, Strugnell W, Doddrell D. The evolution of diffusion anisotropy in ischemic human brain (abstr). In: Proceedings of the Sixth Meeting of the International Society for Magnetic Resonance in Medicine. Berkeley, Calif: International Society for Magnetic Resonance in Medicine, 1998; 1154.
  23. Sorensen AG, Wu O, Copen WA, et al. Human acute cerebral ischemia: detection of changes in water diffusion anisotropy by using MR imaging. *Radiology* 1999; 212:785-792.
  24. Zacharopoulos N, Narayana P. Selective diffusion trace measurements of gray and white matter in human brain with a double-suppression EPI sequence (abstr). In: Proceedings of the Sixth Meeting of the International Society for Magnetic Resonance in Medicine. Berkeley, Calif: International Society for Magnetic Resonance in Medicine, 1998; 664.
  25. Nagesh V, Welch KM, Windham JP, et al. Time course of ADCw changes in ischemic stroke: beyond the human eye! *Stroke* 1998; 29:1778-1782.
  26. Pierpaoli C, Jezzard P, Bassner PJ, Barnett A, Di Chiro G. Diffusion tensor MR imaging of the human brain. *Radiology* 1996; 201:637-648.
  27. Chenevert TL, Brunberg JA, Pipe JG. Anisotropic diffusion in human white matter: demonstration with MR techniques in vivo. *Radiology* 1990; 177:401-405.
  28. Marcoux FW, Morawetz RB, Crowell RM, DeGirolami U, Halsey JH. Differential regional vulnerability in transient focal cerebral ischemia. *Stroke* 1982; 13:339-346.
  29. Brant-Zawadzki M, Atkinson D, Detrick M, Bradley WG, Scidmore G. Fluid-attenuated inversion recovery for assessment of cerebral infarction: initial clinical experience in 50 patients. *Stroke* 1996; 27:1187-1191.
  30. Noguchi K, Ogawa T, Inugami A, et al. MRI of acute cerebral infarction: a comparison of FLAIR and T2-weighted fast spin-echo imaging. *Neuroradiology* 1997; 39:406-410.
  31. Oatridge A, Hajnal JV, Cowan FM, Baudouin CJ, Young IR, Bydder GM. MRI diffusion-weighted imaging of the brain: contributions to image contrast from CSF signal reduction, use of a long echo time and diffusion effects. *Clin Radiol* 1993; 47:82-90.
  32. Bahn MM, Parchi P. Abnormal diffusion-weighted magnetic resonance images in Creutzfeldt-Jakob disease. *Arch Neurol* 1999; 56:577-583.
  33. Carpenter DA, Grubb RL, Powers WJ. Borderzone hemodynamics in cerebrovascular disease. *Neurology* 1990; 40:1587-1592.
  34. Pantoni L, Garcia JH, Gutierrez JA. Cerebral white matter is highly vulnerable to ischemia. *Stroke* 1996; 27:1641-1647.
  35. Kuroiwa T, Nagaoka T, Ueki M, Yamada I, Miyasaka N, Akimoto H. Different apparent diffusion coefficient: water content correlations of gray and white matter during early ischemia. *Stroke* 1998; 29:859-865.
  36. Dewar D, Dawson DA. Changes of cytoskeletal protein immunostaining in myelinated fibre tracts after focal cerebral ischaemia in the rat. *Acta Neuropathol* 1997; 93:71-77.
  37. Yam PS, Dewar D, McCulloch J. Axonal injury caused by focal cerebral ischemia in the rat. *J Neurotrauma* 1998; 15:441-450.
  38. Yenari MA, Palmer JT, Sun GH, de Crespigny A, Moseley ME, Steinberg GK. Time course and treatment response with SNX-111, an N-type calcium channel blocker, in a rodent model of focal cerebral ischemia using diffusion-weighted MRI. *Brain Res* 1996; 739:36-45.
  39. Lo EH, Pierce AR, Mandeville JB, Rosen BR. Neuroprotection with NBQX in rat focal cerebral ischemia: effects on ADC probability distribution functions and diffusion-perfusion relationships. *Stroke* 1997; 28:439-446.
  40. Jiang Q, Zhang ZG, Zhang RL, et al. Diffusion, perfusion, and T2 magnetic resonance imaging of anti-intercellular adhesion molecule 1 antibody treatment of transient middle cerebral artery occlusion in rat. *Brain Res* 1998; 788:191-201.
  41. D'Olhaberriague L, Welch KM, Nagesh V, et al. Preliminary clinical-radiological assessment of a MR tissue signature model in human stroke. *J Neurol Sci* 1998; 156:158-166.